

# The Baroclinic Adjustment of Time-Dependent Shear Flows

FRANCIS J. POULIN

*University of Waterloo, Waterloo, Ontario, Canada*

GLENN R. FLIERL

*Massachusetts Institute of Technology, Cambridge, Massachusetts*

JOSEPH PEDLOSKY

*Woods Hole Oceanographic Institution, Woods Hole, Massachusetts*

(Manuscript received 13 January 2009, in final form 12 March 2010)

## ABSTRACT

Motivated by the fact that time-dependent currents are ubiquitous in the ocean, this work studies the two-layer Phillips model on the beta plane with baroclinic shear flows that are steady, periodic, or aperiodic in time to understand their nonlinear evolution better. When a linearly unstable basic state is slightly perturbed, the primary wave grows exponentially until nonlinear advection adjusts the growth. Even though for long time scales these nearly two-dimensional motions predominantly cascade energy to large scales, for relatively short times the wave-mean flow and wave-wave interactions cascade energy to smaller horizontal length scales. The authors demonstrate that the manner through which these mechanisms excite the harmonics depends significantly on the characteristics of the basic state. Time-dependent basic states can excite harmonics very rapidly in comparison to steady basic states. Moreover, in all the simulations of aperiodic baroclinic shear flows, the barotropic component of the primary wave continues to grow after the adjustment by the nonlinearities. Furthermore, the authors find that the correction to the zonal mean flow can be much larger when the basic state is aperiodic compared to the periodic or steady limits. Finally, even though time-dependent baroclinic shear on an  $f$  plane is linearly stable, the authors show that perturbations can grow algebraically in the linear regime because of the erratic variations in the aperiodic flow. Subsequently, baroclinicity adjusts the growing wave and creates a final state that is more energetic than the nonlinear adjustment of any of the unstable steady baroclinic shears that are considered.

## 1. Introduction

Shear flows with strong spatial gradients are a very important means through which geophysical fluids are able to produce vortical motions that mix physical, chemical, and biological properties. To date, the majority of the literature has focused on studying steady shear flows. The relatively few works that have investigated time-dependent shear flows have almost entirely focused on the extreme cases in which the shear flows are time periodic (Davis 1976) or white noise (Farrell and Ioannou 1996, 1999). Two notable exceptions are Durski et al.

(2008), who recently studied an aperiodic time-dependent coastal upwelling jet, and Inoue and Smyth (2009), who investigated the mixing efficiency of unsteady shear flows. Because the majority of realistic flows lie somewhere between the periodic and white-noise limits, these examples are useful idealizations, but additional research is needed to understand more realistic time-dependent shear flows.

This article investigates the dynamics of time-dependent vertical shear flows that may include erratic variations similar to what is observed in the oceans. Because it is difficult to determine the precise manner in which flows vary in nature, we choose instead to pick a stochastic process that idealizes realistic time variations. In particular, we chose the Kubo oscillator (Gardiner 2004; Risken 1984) because it is a bounded stochastic process that has time-periodic and highly erratic colored noise

---

*Corresponding author address:* Francis J. Poulin, Department of Applied Mathematics, University of Waterloo, Waterloo, ON N2L 3G1, Canada.  
E-mail: fpoulin@uwaterloo.ca

processes at the limits. This type of noise was used in Poulin and Flierl (2008) to study the stochastic Mathieu's equation for internal frequencies with various degrees of stochasticity. The stability analysis determined that, as the internal frequency became slightly aperiodic, the parametric mode (i.e., an instability that arises because of parametric resonance) weakened but persisted for a range of stochasticities. Moreover, we discovered a new type of unstable mode, the stochastic mode, which was found to arise for various types of stochastic processes, thus implying that it is a robust feature.

This work focuses on understanding the stability of time-dependent baroclinic (BC) shear in the context of the Phillips model (Phillips 1951, 1954; Pedlosky 1987). This is a two-layer quasigeostrophic (QG) model on a beta plane, usually in the confines of a zonal channel (Pedlosky 1964a,b). This simple geometry is ideally suited for studying atmospheric flow. The applicability of the Phillips model to the ocean is complicated by the presence of coastal boundaries that can alter the dynamics. The Antarctic Circumpolar Current (ACC) is one part of the ocean where the channel geometry is most applicable (Nowlin and Klinck 1986). The winds in the Southern Ocean provide forcing that can alter the baroclinic shear. The seasonal variations in the winds do not significantly alter the long-term phase of the shear but cause its strength to wander in amplitude. Even though the Kubo oscillator depicts a state that has a random phase, it yields behavior that is similar to one with a varying amplitude. It is for this reason that we suggest our analysis is applicable to the ACC and other examples of baroclinic shear in the ocean. Moreover, the zonal model can also well describe the zonal extensions of both the Gulf Stream and the Kuroshio (Schmeits and Dijkstra 2001).

The spatial and temporal variability in the ACC was studied by Gille and Kelly (1996) using *Geosat* altimeter data. The objective analysis revealed that the ACC had a strong spectral peak at 0.33 cycles per year, but there was also significant variability at much higher frequencies. This suggests that it is of interest to understand the dynamics of baroclinic shear with various spectral peak frequencies. Here, we focus on baroclinic shears that are spatially uniform in the horizontal and have spectral peaks at higher frequencies than the peak that Gille and Kelly (1996) observed. Our goal is not to study the details of the ACC and the effect of the observed spectral peak but instead to understand better the effect that randomness has on baroclinic instability and adjustment in general. It is for this reason that we choose to study time scales on the order of weeks, because these time scales are the easiest to study in the context of the Phillips model. In future works, we will study the effect of randomness

on different time scales, particularly on the longer time scales observed in Gille and Kelly (1996).

In a recent work, Poulin (2010) examined the linear stability of time-dependent baroclinic shear in the context of the two-layer Phillips model on the beta plane where the shear was a Kubo oscillator. He determined that, as the shear becomes more erratic, the growth rates of the parametric mode decrease and the unstable region of parameter space widens. This depicts the dual nature of stochasticity in the linear regime in that it can either stabilize or destabilize the basic state, depending on the particular parameters. In this work, we investigate the nonlinear dynamics of steady, periodic, and aperiodic baroclinic shear flows. In the steady case, the most unstable wave, the primary wave, grows exponentially until it reaches finite amplitude where it is subsequently equilibrated. This nonlinear saturation of exponential growth of a linearly unstable vertical shear is referred to as baroclinic adjustment (Stone 1978). We extend this definition to include the nonlinear saturation that arises because of any vertical shear, whether it is steady or time dependent. The nonlinear processes that achieve this are wave-mean flow and/or wave-wave interactions. Pedlosky (1970) was the first to look at equilibration of a baroclinically unstable steady shear flow resulting from wave-mean flow interactions; since then, there has been a series of works that have extended this idea (Mak 1985; Cai and Mak 1990; Cai 1992).

The outline of this paper is as follows: First, we review the Phillips model and the pseudospectral method used to perform our numerical simulations. Second, we present the nonlinear energy cascades that arise from a classical baroclinic instability (CBI) where the basic state is steady. Even though these types of simulations have been performed frequently, they are useful to present because they facilitate comparisons with the other novel simulations. Third, we study the baroclinic adjustment of time-dependent flows whose mean shear is subcritical or supercritical because there are examples of both throughout the ocean. The only study that we are aware of that has investigated the nonlinear energy cascade as a result of a parametric instability (PI) is Flierl and Pedlosky (2007). They choose to look at the energy partition between the low wavenumbers (mode one and two) and the higher wavenumbers (mode three and higher). We focus instead on several of the largest modes that fit in our domain to learn how their baroclinic adjustment transfers energy to the smaller length scales. Fourth, we do a similar analysis for aperiodic baroclinic shears on a  $\beta$  plane and contrast this with their periodic analogs. Fifth, we investigate the nonlinear evolution of aperiodic baroclinic shear on an  $f$  plane that is linearly stable. Sixth, we show how the different simulations

generate mean flow corrections to the basic state and finally summarize our findings.

## 2. The model equations

To study large-scale time-dependent baroclinic shears in the ocean, we use the two-layer Phillips model because it has had some success in modeling the onset and nonlinear saturation of the instability of some mesoscale oceanic jets (Charney and Flierl 1981). We assume that the geometry is a periodic zonal channel of width  $L$  and length  $2L$  on a  $\beta$  plane with external forcing that maintains the time-dependent basic state (Flierl and Pedlosky 2007). The governing equations assume the standard nondimensionalization in QG theory:  $L$  and  $D$  are the horizontal and vertical length scales,  $U_{\text{dim}}$  and  $U_{\text{dim}}D/L$  are the horizontal and vertical velocities, the time scale is advective, and the scaling for pressure is geostrophic (Pedlosky 1970). The Coriolis parameter is  $f = f_0 + \beta_{\text{dim}}y$ , and the reduced gravity between the two layers is  $g'$ . This allows us to define the two nondimensional parameters, the Froude number  $F$  and the nondimensional  $\beta$  parameter:

$$F = \frac{f_0^2 L^2}{g' D} \quad \text{and} \quad \beta = \frac{\beta_{\text{dim}} L^2}{U_{\text{dim}}}. \quad (1)$$

If we use  $G_n(y, t)$  to denote the forcing that maintains the time-varying shear, the equations that determine the evolution of the system are

$$\frac{\partial q_n}{\partial t} + J(\psi_n, q_n) + \beta \frac{\partial \psi_n}{\partial x} = G_n(y, t), \quad \text{for } n = 1, 2, \quad (2)$$

where the potential vorticities (PVs)  $q_n$  and the streamfunctions  $\psi_n$  are related as

$$q_n = \nabla^2 \psi_n + (-1)^n F(\psi_1 - \psi_2), \quad \text{for } n = 1, 2, \quad (3)$$

and the velocities in each layer are

$$(u_n, v_n) = \left( -\frac{\partial \psi_n}{\partial y}, \frac{\partial \psi_n}{\partial x} \right). \quad (4)$$

Note that  $J$  is the Jacobian operator and the subindices 1 and 2 denote the upper and lower layers, respectively. We restrict our attention to the case of equal layer depths  $D$ , but in future studies the importance of varying layer depths will be considered. Even though there are many damping mechanisms in the ocean, we choose to investigate the conservative version of Eq. (2) because it produces the most energetic energy cascades. Although

dissipation may affect the long time behavior of the dynamics, we have considered only a simpler conservative system to focus on the inviscid energy cascade. The model uses a spectral filter to dampen the small-scale structure; it does play a significant role in the enstrophy budget.

We use  $U_n(t)$ ,  $U_m$ , and  $U_s(t)$  to denote the zonal velocity in each layer for  $n = 1$  and 2, the mean velocity and half of the shear between the two layers, respectively:

$$U_m = \frac{1}{2}[U_1(t) + U_2(t)] \quad \text{and} \quad (5)$$

$$U_s(t) = \frac{1}{2}[U_1(t) - U_2(t)]. \quad (6)$$

Because we are interested in studying baroclinic effects, we only consider flows where  $U_m$  is constant. This implies that we are restricting our attention to flows with constant across channel transport. Therefore, the streamfunction and PV associated with the basic state are

$$\Psi_n = -U_n y \quad \text{and} \quad (7)$$

$$Q_n = (-1)^n F(U_1 - U_2)y, \quad (8)$$

and the particular forcing required to maintain this flow is

$$G_n(y, t) = (-1)^n F \left( \frac{dU_1}{dt} - \frac{dU_2}{dt} \right) y. \quad (9)$$

Physically, this forcing could be attributed to the winds and/or buoyancy effects. Our model implicitly assumes that the atmosphere is passive in that it forces the ocean but does not respond to the ocean. A more detailed study could look at the coupled atmosphere–ocean interactions to investigate how they evolve, but this is beyond the scope of this work.

We idealize the forcing to be a Kubo oscillator (Gardiner 2004; Risken 1984) because it is easy to generate and can produce baroclinic shears with a wide range of temporal variations. In particular, the functional form of the shear is set to be

$$U_s(t) = g_0 + h_0 \cos \left[ \frac{2\pi t}{T} + \sigma \int_0^t \eta(s) ds \right], \quad (10)$$

where the Kubo oscillator is the sinusoidal portion of the equation. The parameters  $g_0$  and  $h_0$  determine the mean component and fluctuating components of the flow, respectively. The parameters  $T$  and  $\sigma$  are the mean period and level of stochasticity. The function  $\eta(t)$  is Gaussian white noise and its integral is a Wiener process (Gardiner 2004).

The Kubo oscillator is a bounded function that in one limit,  $\sigma = 0$ , is a cosine and the other limit,  $\sigma \rightarrow \infty$ , is highly variable colored noise. For all other values of  $\sigma$ , we have an oscillatory-like function that is erratic, the degree of which is determined by the magnitude of  $\sigma$ . The power spectrum of the Kubo oscillator is a delta function at  $\sigma = 0$ ; as  $\sigma$  increases, the width of the peak broadens tending to a uniform distribution. Alternatively, because of the functional form of Eq. (10), one can interpret  $\sigma$  as controlling the time-varying phase of the noise. In the literature on stochastic processes, this term has been referred to as the phase diffusion because the phase is allowed to wander in time (Van Kampen 2001; Gleeson 2006; Talkner et al. 2005). Details on particular realizations of this type of noise and its spectrum can be found in Poulin and Flierl (2008) and Poulin (2010).

We define the perturbation streamfunction and PV from the basic state to be  $\psi'_n$  and  $q'_n$ , respectively:

$$\psi_n = U_n(t)y + \psi'_n \quad \text{and} \quad (11)$$

$$q_n = Q_n + q'_n. \quad (12)$$

The numerical method that we employ to integrate the fully nonlinear equations to compute the evolution of the perturbation is the same as used in Flierl and Pedlosky (2007). It is a pseudospectral method that solves the two equations for the perturbation potential vorticity  $q'_n$  and mean zonal velocity  $U_n$ :

$$\begin{aligned} \frac{\partial}{\partial t} q'_n + \frac{\partial}{\partial x} (U_n q'_n + u'_n q'_n) + \frac{\partial}{\partial y} (v'_n q'_n - \overline{v'_n q'_n}) \\ + \left( \frac{\partial Q_n}{\partial y} + \beta \right) v'_n = 0 \quad \text{and} \end{aligned} \quad (13)$$

$$\frac{\partial}{\partial t} U_n - \overline{v'_n q'_n} = (-1)^{n+1} F\phi, \quad (14)$$

where

$$q'_n = \nabla^2 \psi'_n + (-1)^n F(\psi'_1 - \psi'_2), \quad (15)$$

$$(u'_n, v'_n) = \left( -\frac{\partial \psi'_n}{\partial y}, \frac{\partial \psi'_n}{\partial x} \right), \quad (16)$$

and the overbar denotes the zonal average. The function  $\phi$  in the equation for the zonal mean flow is related to the transformed Eulerian-mean meridional circulation defined in Shepherd (1983) and Flierl and Pedlosky (2007) and satisfies the following equation:

$$f_0 \overline{v_n^*} = (-1)^n F\phi. \quad (17)$$

### 3. Numerical method and parameters

We use numerical simulations to explore the nonlinear dynamics of time-dependent baroclinic shear flows for a range of mean shears  $g_0$ , amplitude of oscillations  $h_0$ , and stochasticities  $\sigma$ . The channel geometry has an aspect ratio of 2 to 1 with 128 and 64 points in the  $x$  and  $y$  directions, respectively. The code is initiated with two second-order Runge–Kutta steps and subsequently uses the third-order Adams–Bashforth scheme. Even though this mesh is relatively coarse compared to other studies, the exponential convergence of the spectral method allows for very accurate resolution of a wide range of length scales. This saving in computational time enabled us to do many calculations to explore an array of parameters. Our aim is not to explore all of parameter space but instead to focus on several interesting cases to better understand the various characteristics that can arise because of the different instability mechanisms.

In each simulation, we perturb the basic state with a random field that is very small in amplitude. In the early stages, the most unstable mode (primary mode) grows exponentially by extracting energy from the basic state. This continues until the amplitude of the unstable mode is comparable to that of the basic state, and then nonlinear effects become important. Subsequently, the nonlinearities equilibrate the growth of the primary wave and, because of wave–mean flow and wave–wave interactions, transfer energy to harmonic waves that grow in amplitude. This nonlinear energy cascade continues to distribute energy over a vast range of length scales, producing a broad energy spectrum. The richer the energy spectrum, the more chaotic the solution. In all of our simulations the most unstable mode has a wave vector of  $(k, l) = (1, 1)$  (nondimensional wavenumber vector), the largest mode that fits in the channel geometry. In similar calculations that integrated the solution for a long time, it was determined that the dynamically most efficient wave (i.e., the wave responsible for the most baroclinic adjustment) has a longer wavelength than the primary wave (Mak 1985; Cai and Mak 1990; Cai 1992). These waves are not permitted in our model, because the domain size does not allow waves larger than the most unstable mode.

The essential reason why spectral methods are computationally efficient is because of the fast Fourier transform that allows us to compute the spectral decomposition of any field very quickly (Press et al. 2007). Our numerical method decomposes the solution in the zonal and meridional directions using the Fourier and Fourier sine transforms, respectively. To do the latter, it is necessary to use the odd extension of the streamfunction. Because of this discrepancy, mode one in the zonal direction

corresponds to a full sine wave whereas mode one in the meridional direction is half of a sine wave. Even though it is very easy to compute the time series for each mode, graphically it is very difficult to display all this information simultaneously. Thus, we have chosen instead to focus on the first evolution of the following modes: (1, 1), (2, 1), (1, 2), and (2, 2). Many other waves are included in the calculations because they are important in the adjustment process.

#### 4. Steady baroclinic shear flow

Throughout this work, we investigate the different spectral characteristics that arise because of various types of baroclinic shear. To begin, we superimpose a small-amplitude random perturbation on the basic state and then let it evolve freely to discover how the nonlinearities baroclinically adjust the instabilities that develop. The most unstable mode always has a mode-one structure in the meridional direction. Unless otherwise stated, it is assumed that  $F = 20$  and  $\beta = 20$ . For these parameters, it has been shown in Poulin (2010) that the critical value for instability in nondimensional units is  $U_c = 0.5825$ . The primary wave (1, 1) is the only linearly unstable mode, and it grows exponentially until it is eventually saturated by nonlinear effects. In this adjustment process, the mode (2, 2) is generated and grows rapidly because of wave–wave self interactions of the primary wave. Then, the (2, 2) waves saturate; soon afterward, we have other modes that are generated [e.g., (2, 1) and (1, 2); shown in Fig. 2]. The saturation level of the (2, 2) modes are lower than that of the primary wave. Other modes are generated at this stage, but their amplitudes are smaller than that of the primary wave. During the adjustment process, there is an equilibrated mean flow that is created with meridional variation that allows for a variety of wave–mean flow interactions.

We first discuss the nonlinear equilibration that takes place as a result of steady supercritical vertical shears. Even though the nonlinear evolution of baroclinic instability has been extensively studied in the literature, we present these results to compare and contrast them with the baroclinic adjustment that arises from time-dependent baroclinic shear that appears in the following sections. Figures 1 and 2 plot the amplitude of the Fourier coefficient of the barotropic (BT) and BC components of the growing modes. Figures 1a,b and 2a,b depict the growth of the modes (1, 1), (2, 2), (2, 1), and (1, 2), respectively. Each subplot is divided into three columns, each of which displays a different type of instability: the left is a CBI (with  $h = 0$  and  $g = 0.6, 0.7, 0.8$ , and  $0.9$ ), the middle is a PI (with  $h = 0.1$  and  $g = 0.2, 0.3, 0.4$ , and  $0.5$ ), and the right is a mixed CBI and PI (with  $h = 0.1$  and

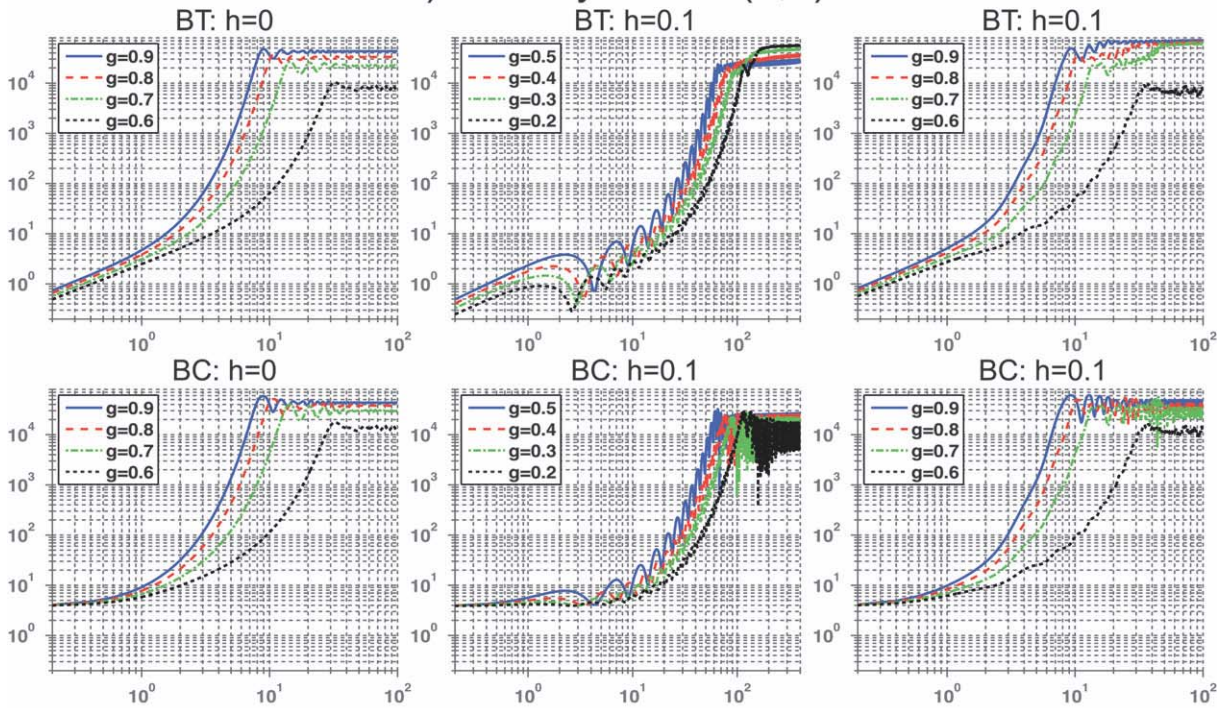
$g = 0.6, 0.7, 0.8$ , and  $0.9$ ). The top subplot in each column is divided into BT and BC components. We have chosen to plot all of these figures together to facilitate the comparison between the different instability mechanisms. A log scale is used on both axes because of the large variation of length scales throughout the simulations.

In the plots of the growth of the primary wave in each of the four cases, it is readily observed that the rate of exponential growth increases with the degree of supercriticality of the basic state, as is well known. Upon close inspection, it can be verified that the slightly supercritical flows have more energy in the baroclinic mode, as predicted by the linear theory (Pedlosky 1987); however, as  $g_0$  increases, the energy is more evenly distributed. For  $g_0 = 0.9$ , the primary baroclinic wave achieves a larger amplitude and possesses stronger oscillations before equilibrating. Also, as the harmonic wave (2, 2) extracts energy from the primary wave, it grows much faster than the primary wave. The level of equilibration tends to increase with increasing  $g_0$ ; however, the barotropic component of the harmonic wave with  $g_0 = 0.9$  equilibrates at a lower level than the flows with  $g_0 = 0.7$  and  $0.8$  and oscillates more rapidly and with a larger amplitude than the three other examples of CBI. The (2, 1) and (1, 2) waves plotted in Fig. 2 increase in amplitude at a rate in between the (1, 1) and (2, 2) modes. The levels of equilibration of these waves are comparable to the case with  $g_0 = 0.6$  because it has only started to grow. The interested reader is directed to the following works on wave–wave interactions in baroclinic shear and the citations within for further details: Klein and Pedlosky (1986), Pedlosky and Polvani (1987), Klein (1990), and Pierrehumbert (1995).

#### 5. Periodic baroclinic shear flow

In this section, we extend our investigation of nonlinear energy cascade to periodic baroclinic shears. The examples we consider are different from those studied in Flierl and Pedlosky (2007), as is our focus, because we investigate how energy is transferred among the different modes after baroclinic adjustment has occurred. First, we pick vertical shears in the Phillips model whose mean is subcritical of the steady criteria for instability. We choose small-amplitude oscillations,  $h_0 = 0.1$ , with mean shears of  $g_0 = 0.2, 0.3, 0.4$ , and  $0.5$  and periods of  $T = 3, 3, 3.5$ , and  $4$ , respectively. Note that all of these shear flows are subcritical at each instant of the classical criteria for stability, except the simulation with  $g_0 = 0.5$  that only slightly exceeds it for a brief interval of time in each period. The different periods are chosen to ensure that we are in a regime where the vertical shear is parametrically unstable. These periods are determined using

a) Primary Wave: (1,1)



b) First Harmonic: (2,2)

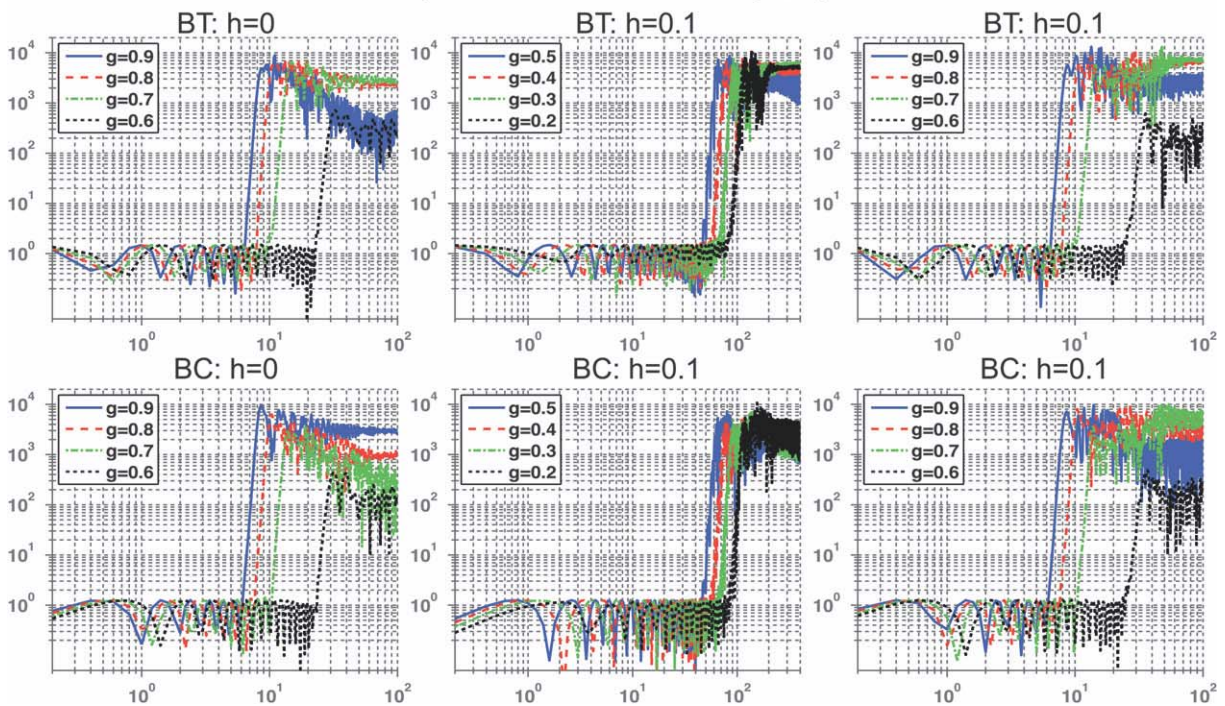
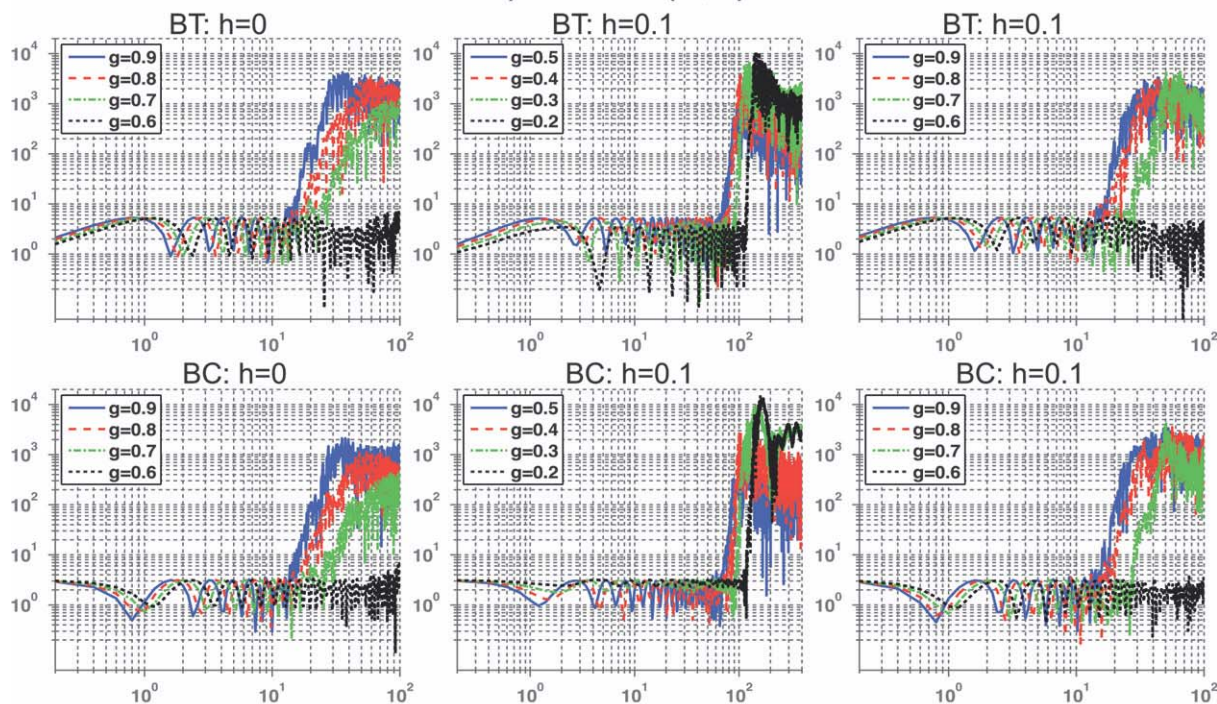


FIG. 1. Plots of the energy of the BT and BC components of the growing modes with  $F = 20$ ,  $\beta = 20$  for (a) the primary wave (1, 1), and (b) first harmonic (2, 2). The subplots are organized in pairs for (top) BT and (bottom) BC components, for (left) a CBI with  $h = 0$  and  $g = 0.6, 0.7, 0.8$ , and  $0.9$ ; (middle) a pure PI with  $h = 0.1$  and  $g = 0.2, 0.3, 0.4$ , and  $0.5$ ; and (right) a mixed CBI and PI with  $h = 0.1$  and  $g = 0.6, 0.7, 0.8$ , and  $0.9$ .

a) Mode: (2,1)



b) Mode: (1,2)

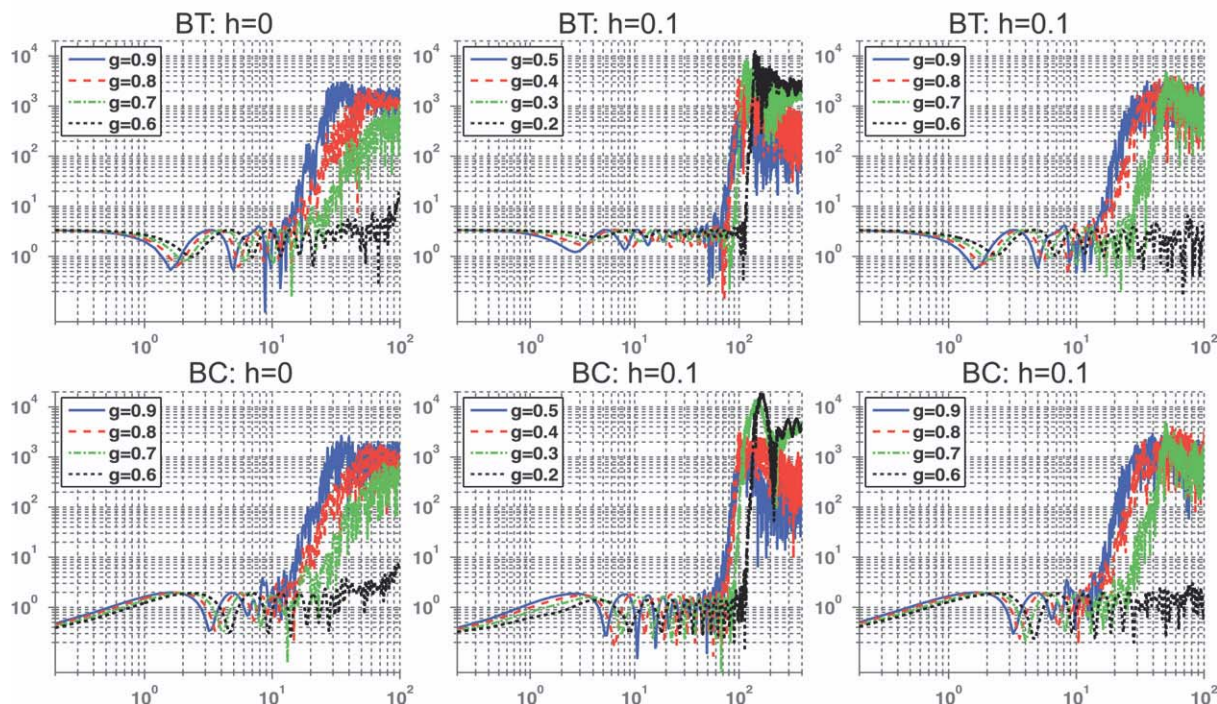


FIG. 2. As in Fig. 1, but for (a) mode (2, 1), and (b) mode (1, 2).

the contour plots of Poulin (2010) that depict the regions of parametric instability in the linear regime. Given that the dimensional time scale is the advective time scale, these periods are on the order of several days to weeks.

The second column of plots in Figs. 1 and 2 present the time evolution of the first several modes in the four different cases mentioned previously. Because the mean flows are subcritical of the steady criteria for instability, they are not examples of CBI but instead are examples of PI. Both instabilities are due to a resonant triad that is established between the barotropic and baroclinic components of the primary wave and the mean flow. The essential difference is that in PI the mean flow is periodic (Pedlosky and Thomson 2003; Poulin et al. 2003), whereas in CBI the mean flow is steady. This subtle difference is significant, because PI has an infinite number of unstable modes, whereas in CBI there is usually one or perhaps several unstable modes that fit within a channel domain.

One commonality between the simulations of CBI and PI is that the rate of growth of each particular wave increases with the parameter  $g_0$ . However, in PI both components of the growing primary waves oscillate, unlike in CBI. One important difference is that, in the simulation with  $g_0 = 0.2$ , which has a relatively slow growing primary wave, in the saturation phase the barotropic component equilibrates at the highest level to all the other cases in these two figures. This is in contrast to the baroclinic component of the primary wave that is significantly weaker in PI than in CBI. As the mean shear increases, the equilibration level of the barotropic component decreases. A crucial difference in PI is that the modes (2, 1) and (1, 2), which are less energetic compared to (1, 1) and (2, 2), have larger magnitudes than what was observed in CBI by an order of magnitude. This reveals that PI tends to excite a wider range of modes more rapidly than what is achieved in CBI.

Next, we study the baroclinic adjustment of oscillatory vertical shear in the Phillips model, whose mean is supercritical. PI only happens for a limited range of periods and the smaller the amplitude of the oscillation, the smaller the range of unstable parameters. It was shown in Poulin (2010) that, as the period increases, the growth rates of PI decreases and the level of saturation is the same as was observed in CBI. The results from these simulations are in the third column of Figs. 1 and 2, and the following features are observed: First, the exponential growth of the primary wave is not significantly altered by the presence of a small-amplitude oscillation. However, the equilibration levels differ significantly from the first to the third columns. The larger the supercriticality, the larger the levels of saturation of the primary waves in comparison to CBI. Therefore, the presence of oscillations in the basic state plays an influential role in

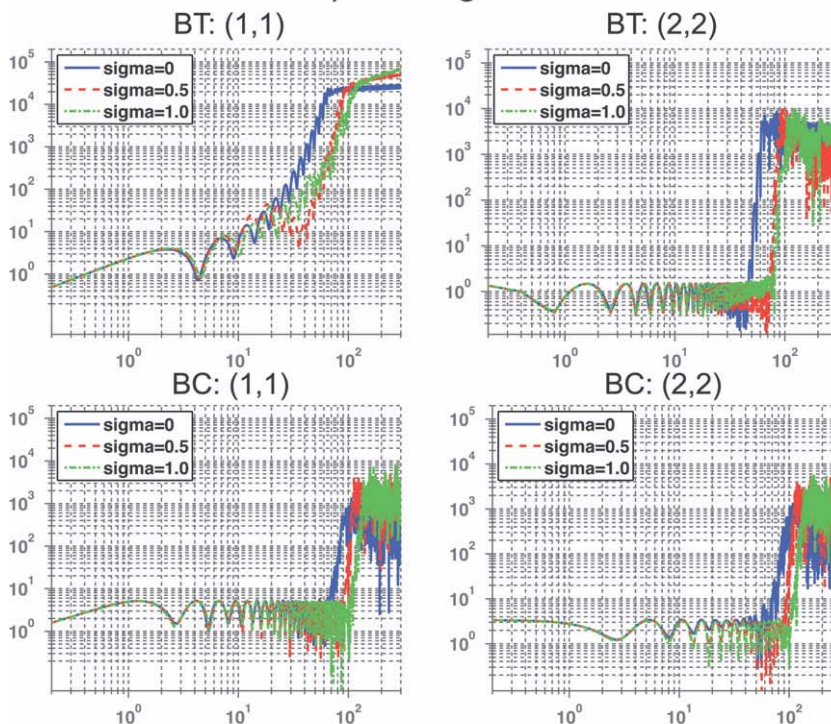
the baroclinic adjustment phase by allowing the barotropic component to achieve a higher energy level. Second, the harmonic modes in the third column contain more energy than in the first column. Therefore, in these four simulations, the destabilization of the primary wave is almost entirely due to CBI, but then there is a weak secondary instability due to PI that further excites the primary wave and its harmonics.

## 6. Aperiodic baroclinic shear flow

After having studied typical examples of steady and periodic baroclinic shear and the nonlinear energy transfer that ensues at the early stages of baroclinic adjustment, we are now in a position to study the more complex problem of aperiodic baroclinic shear to learn what effects aperiodicity has on the nonlinear energy transfers. We choose two sets of parameters: one has a mean baroclinic shear that is subcritical ( $h = 0.1$  and  $g = 0.5$ ) and the other has a mean shear that is slightly supercritical ( $h = 0.1$  and  $g = 0.6$ ). Note that in both cases the amplitude of the shear is relatively small in comparison to the shear itself. In Figs. 3a,b, we plot the evolution of the amplitude of the Fourier coefficients of the BT and BC components of the perturbation as computed from the two sets of simulations with  $\sigma = 0, 0.5$ , and  $1.0$ . Even though the periodic calculations have already been presented, they are duplicated here to facilitate comparison of the instabilities that arise from periodic and aperiodic baroclinic shear. We subsequently refer to the cases with  $\sigma = 0.5$  and  $1.0$  as mild and moderate levels of stochasticity, respectively. In Fig. 3a, the first column shows the barotropic and baroclinic components for the primary wave, whereas the second column is the same but for the first harmonic that is generated from baroclinic adjustment. Figure 3b is analogous, but the two columns correspond to the modes (2, 1) and (1, 2), respectively. Each column in this figure depicts the energy of a particular mode for a single realization of aperiodic shear flow and therefore we cannot generalize to say that these characteristics must always occur. However, we considered several different realizations and the results presented here are typical of our relatively small ensemble. These simulations were performed to idealize oceanographic (and some atmospheric) baroclinic shear flows that are near criticality with a significant but small-amplitude disturbance that is aperiodic but still somewhat regular.

There are several important results that can be deduced from this figure. First, the presence of randomness decreases the exponential growth rates of the primary wave. The fact that sufficiently strong randomness ( $\sigma$  large enough) can quench the linear instability is very

a)  $h=0.1$   $g=0.5$



b)  $h=0.1$   $g=0.6$

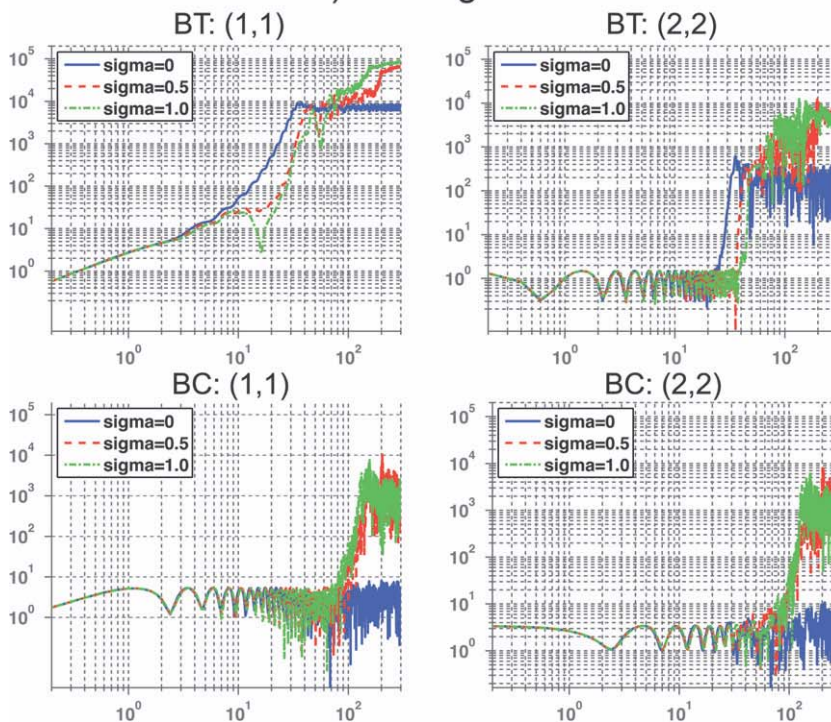


FIG. 3. Plots of the energy of the BT and BC components of the perturbation with  $F = 20$ ,  $\beta = 20$ ,  $g = 0.6$ , and  $h = 0.1$  for  $\sigma = 0, 0.5$ , and  $1.0$ . The first basic state is periodic and is provided for reference. The second and third have background flows that possess mild and moderate levels of stochasticity. (a)  $h_0 = 0.1$  and  $g_0 = 0.6$  and (b)  $h_0 = 0.1$  and  $g_0 = 0.6$ . The subplots are for the waves (left) (1, 1) and (right) (2, 2), for the (top) BT and (bottom) BC energies.

important, because this means that the basic flow must be sufficiently well behaved in time to allow for an instability and a turbulent cascade. Figure 4 of Poulin (2010) presents the growth rates for the linear stability of aperiodic baroclinic shear. It clearly shows that, when the erratic component of the baroclinic shear is large enough, the growth rate of the basic state is equal to that of its time average. This demonstrates that PI cannot manifest itself unless the basic state is close to periodic. This is why we cannot study baroclinic adjustment for a wide range of values of  $\sigma$ , because when  $\sigma$  is large enough the instability mechanism can be suppressed. Second, baroclinic adjustment takes place when the perturbations become finite amplitude and wave–wave and wave–mean flow interactions are then possible. This excites a wider range of modes than in the periodic or steady limits. However, unlike in the steady and periodic scenarios, the barotropic component of the primary wave does not saturate and continues to grow to become very large in amplitude. The baroclinic components do saturate but at a higher level than in the periodic case and oscillate more irregularly with larger amplitudes. The end result is that the barotropic component of the primary wave is dominant for the remainder of the simulation. The growth is stronger for the supercritical scenarios. Third, because the primary wave continues to extract energy from the background flow, the harmonics and other modes can acquire more energy and also grow to be much larger in amplitude. Fourth, by comparing the energy in the primary barotropic mode with mild and moderate stochasticities, it is readily seen that the dominance of the barotropic component of the primary wave resulting from an aperiodic basic state is enhanced with increasing values of  $\sigma$ . The primary wave and its harmonics have higher energy levels because of the coupling of both CBI and PI in the vertical shear up to a point; beyond that point, the flow can be completely stabilized.

## 7. Aperiodic baroclinic shear flow on the $f$ plane

Flierl and Pedlosky (2007) showed that the growth rates of any periodic baroclinic background shear on the  $f$  plane is equal to that of the time average of the shear. More recently, Poulin (2010) extended this result to demonstrate that it applies to any time-dependent baroclinic shear with zero mean. However, Flierl and Pedlosky (2007) verified through nonlinear simulations that, if the initial amplitude of the perturbation is large enough, the basic state is subject to a nonlinear instability. The linear stability of these states is perhaps surprising, given that the flow is supercritical for some intervals of time for any level of the shear.

In this section, we investigate the nonlinear evolution of aperiodic baroclinic shear on an  $f$  plane. In Fig. 4, we plot the time evolution of the first several Fourier coefficients for the case of  $F = 20$ ,  $\beta = 0$ ,  $g_0 = 0$ ,  $h_0 = 0.25$ ,  $\sigma = 2.0$ , and  $T = 3$  up to  $t = 300$  nondimensional units. Unlike all the previous manifestations of instability, in this simulation there is no indication of exponential growth. The (1, 1) wave, which we can no longer refer to as the primary wave because it is not linearly unstable, increases in energy in a rather erratic and strongly non-monotonic fashion. In the four subplots, this wave is the most energetic and achieves large enough amplitudes that nonlinear adjustment takes place even though the wave is linearly stable. In the phase of baroclinic adjustment, wave–wave self interactions generate the (2, 2) wave that grows to be very strong in amplitude as well. The (2, 1) and (1, 2) waves only start to get excited near the end of the simulation, but many other modes are excited as well. As a result, at the final time, the solution has a very broad spectrum of waves. Throughout, there does not appear to be a significant difference in the amplitude of the barotropic and baroclinic components.

To better understand the structure of the growing nonlinear instability, in Fig. 5 we present snapshots of the barotropic and baroclinic potential vorticity fields for this simulation at the nondimensional times of  $t = 205$ , 213, 236, and 330. Figure 5a shows that, at time  $t = 205$ , the mode-one component of the fastest growing mode is clear and strongly established. Previously, there were instances when the same structure appeared but then disappeared soon afterward. As explained in Poulin (2010), for an instability to occur on the  $f$  plane, it is necessary that the vertical shear is uniform in sign for long enough that the perturbations grow and enter the nonlinear regime. Because the shear varies in an erratic fashion, this is bound to happen eventually, but it may take a very long time for it to materialize.

Figure 5b plots the PV at  $t = 213$  and shows that there are other harmonics present because there is a clear asymmetry in the meridional direction. None of the other simulations we presented had any noticeable asymmetry early on. Previous to this time, the (1, 1) wave grew and then decayed in amplitude. This loss of energy could have contributed to the growth of the first harmonic as a result of nonlinear self interactions of the (1, 1) wave. Indeed, Fig. 4 indicates that the second strongest mode at time  $t = 213$  is the (2, 2) wave, and this structure is consistent with the mode-two structure observed in the second frame. Therefore, the image at  $t = 213$  is a combination of a strong (1, 1) wave and a (2, 2) wave.

At the third time,  $t = 236$ , the solution must have significant nonlinear effects because the amplitude of the perturbations is on the order of 0.4. The roll up of the

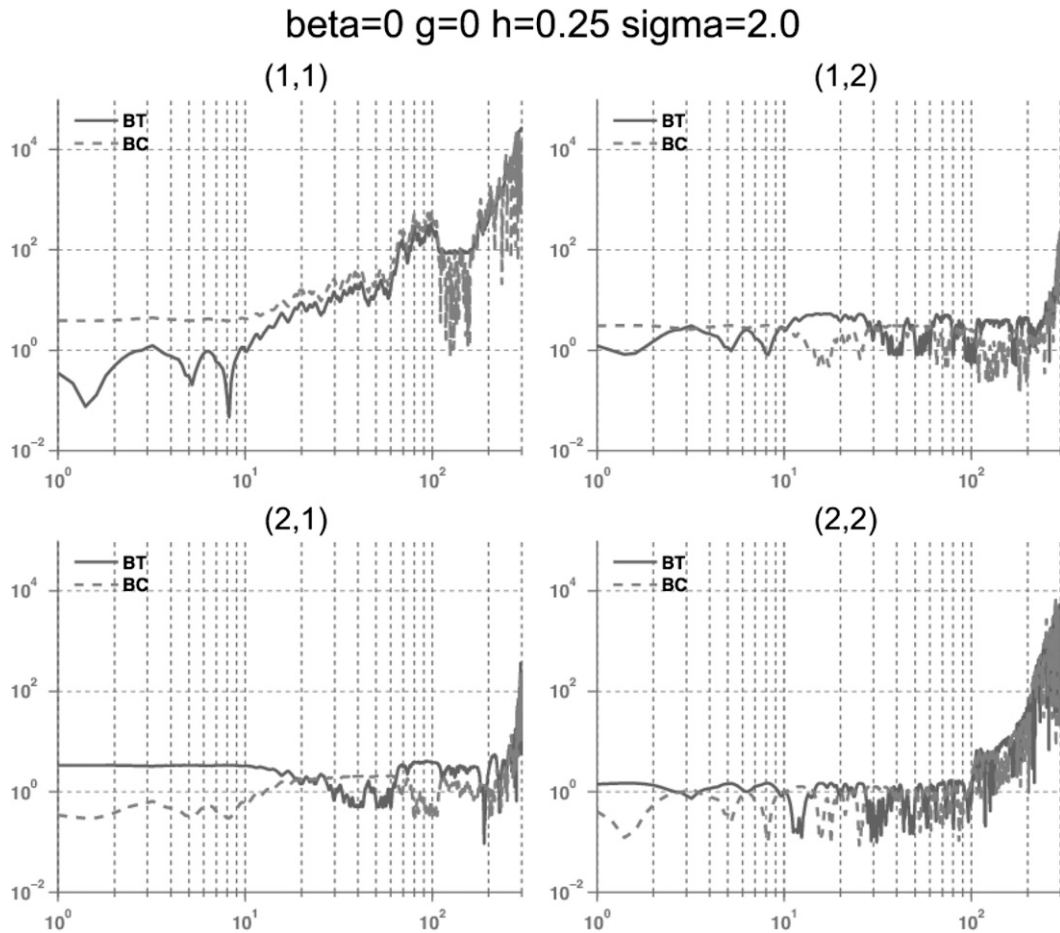


FIG. 4. Plots of the energy in the BT and BC components of the unstable perturbation of an aperiodic BC shear on an  $f$ -plane with  $F = 20$ ,  $g_0 = 0$ ,  $h_0 = 0.25$ ,  $\sigma = 2.0$ , and  $T = 3$ . The subfigures plot the energy of the modes for the waves (1, 1), (1, 2), (2, 1), and (2, 2).

modes at this stage is a result of wave breaking and was not observed in any of our simulations that were linearly unstable. This leads to the final image at  $t = 330$  that consists predominantly of the primary wave but with many filament structures. These filaments are due to the strong presence of higher harmonics in the end state. From this, we gather the following insight: Even though  $f$ -plane dynamics is linearly stable, the aperiodicity of the basic state generates a much more chaotic end state because of the absence of baroclinic adjustment. This can be attributed to the fact that the disturbances that are generated do not propagate away from the source because the group speed is zero, and this enables the energy to build up in a given location and thus create a more turbulent state.

### 8. Mean flow corrections on the $\beta$ plane

It has long been appreciated that the process of baroclinic adjustment generates a mean flow that, in addition

to altering the basic state, can contribute to the wave–mean flow interactions and thus further enhance the turbulent energy cascade. In Figs. 6a,b, we present the equilibrated mean flow from our simulation of unstable steady baroclinic shear with  $g_0 = 0.6$ ,  $h_0 = 0.0$ , and  $\sigma = 0.0$ . In each figure, the top and bottom panels correspond to the barotropic and baroclinic mean flow, respectively, that is generated. Figure 6a focuses on the initial adjustment process, whereas Fig. 6b looks at a later interval of time after the perturbations have been equilibrated. The zonal barotropic velocity that is induced has a mode-three structure that reaches its maximum amplitude near  $t = 35$  and then decreases in magnitude. This equilibrated flow oscillates in amplitude but persists for all time. The baroclinic portion of the zonal flow is similar, except the structure is predominantly mode one in the meridional direction. In the long time evolution, the baroclinic component of the generated mean flow is larger in amplitude in comparison

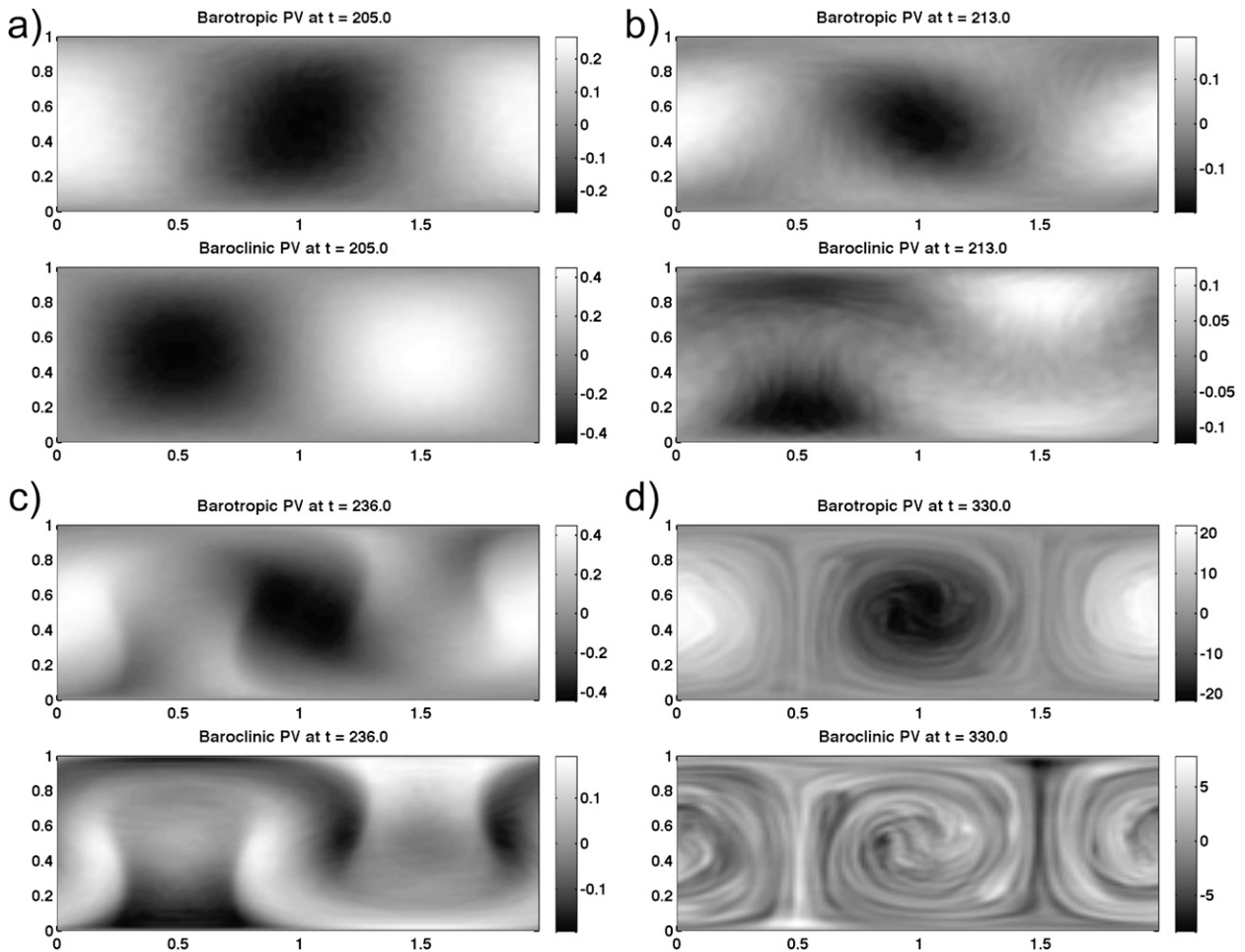


FIG. 5. Snapshots of the fully nonlinear perturbation PVs of an aperiodic BC shear on an  $f$  plane with  $F = 20$ ,  $g_0 = 0$ ,  $h_0 = 0.25$ ,  $\sigma = 2.0$ , and  $T = 3$  at the four different times of  $t =$  (a) 205, (b) 213, (c) 236, and (d) 330. The top and bottom panels in each pair are the BT and BC modes, respectively.

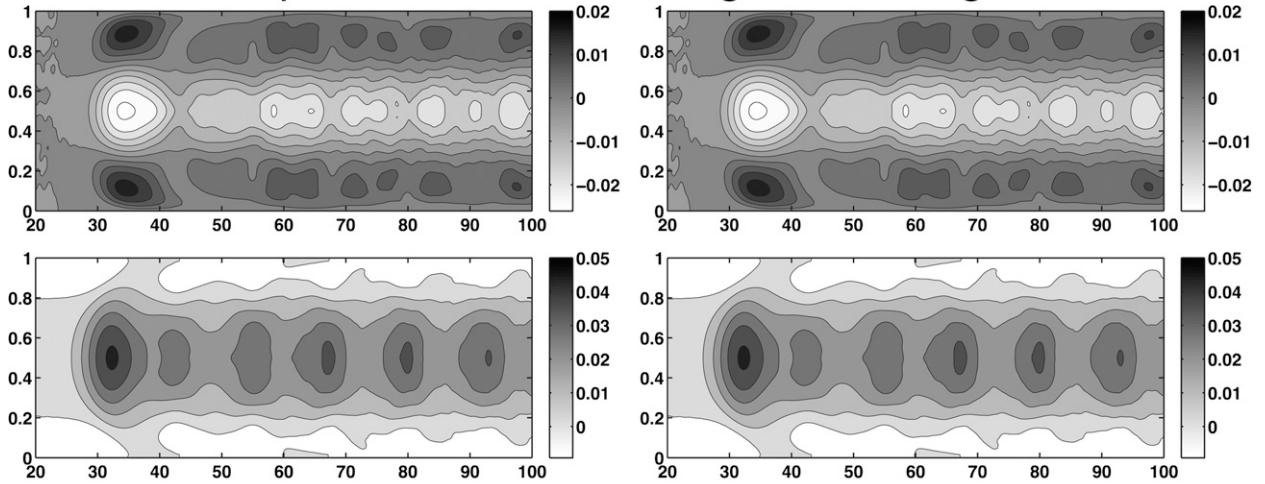
to the barotropic part. In this scenario, the mean shear is only slightly supercritical; consequently, the amplitude of the equilibrated shear is very small. In the other cases of CBI that we have considered (not shown here), we found that, if the mean baroclinic shear increases in strength, the resulting mean flows were similar but larger in magnitude. Interestingly, in CBI the equilibrated mean flow achieves its maximum at the early stages of equilibration. Subsequently, the wave–mean flow interactions transfer energy from the equilibrated flow to various waves, leaving a much weaker mean flow.

In contrast to Flierl and Pedlosky (2007), who looked at how the equilibrated mean flow resulting from a periodic baroclinic shear depends on the nondimensional parameters, we instead investigate how the mean flow varies temporally. In Figs. 6c,d, we plot the barotropic and baroclinic mean zonal flow corrections (organized as before) with  $g_0 = 0.2$ ,  $h_0 = 0.1$ , and  $\sigma = 0.0$ ; this basic

state is at every instant subcritical of CBI. Initially, both the barotropic and baroclinic components of the equilibrated flows grow but in a manner that is far different than CBI. In the early stages of adjustment, both the barotropic and baroclinic components have a mode-three meridional structure superimposed with oscillations. The equilibrated flow is much stronger in amplitude in comparison to CBI, as are the relative amplitude of the oscillations, and each component is comparable in magnitude. For larger values of the mean baroclinic shear approaching criticality, the equilibrated baroclinic shear tends to become larger than the barotropic one and both mean flows are more irregular. In these cases, the dominance of the baroclinic field is presumably due to the fact that there are instances where the basic state is supercritical and thus occasionally subject to CBI.

Figures 7a,b present the equilibrated zonal mean shear for a periodic basic state whose mean is slightly

### Equilibrated Mean Flow: $g=0.6$ $h=0$ $\sigma=0$



### Equilibrated Mean Flow: $g=0.2$ $h=0.1$ $\sigma=0$

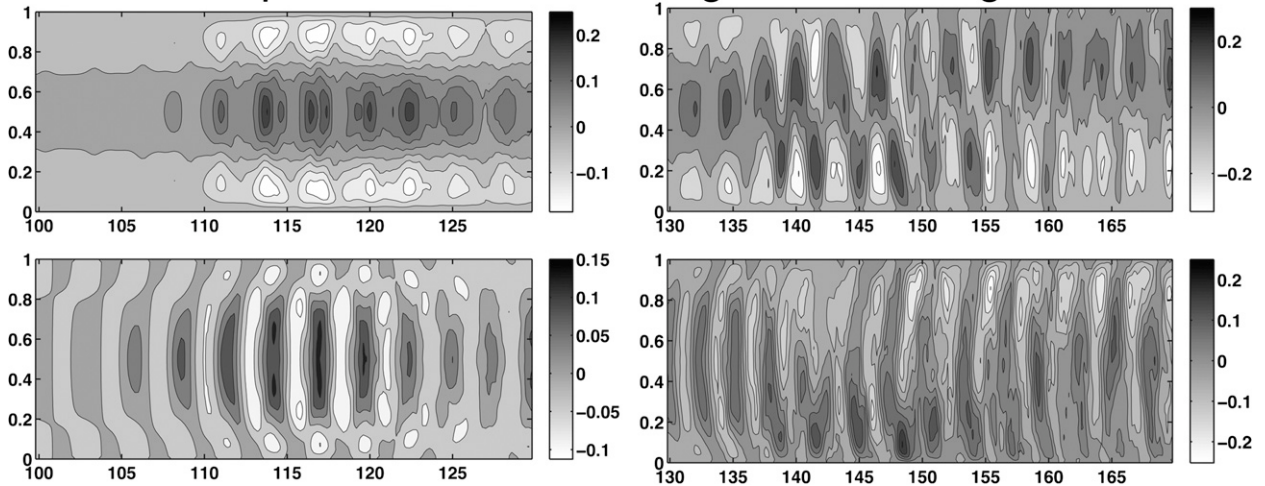


FIG. 6. Plots of the equilibrated zonal flow resulting from BC adjustment: (top) focuses on an example where the basic state is steady ( $g_0 = 0.6, h_0 = 0.0, \sigma = 0.0$ ); the left panel looks at early times and the right focuses on later times. The top and bottom plots in each quadrant are the BT and BC mean flow corrections, respectively. (bottom) As in (top), but for a periodic basic state far from criticality, with  $g_0 = 0.2, h_0 = 0.1$ , and  $\sigma = 0.0$  and structured in the same way.

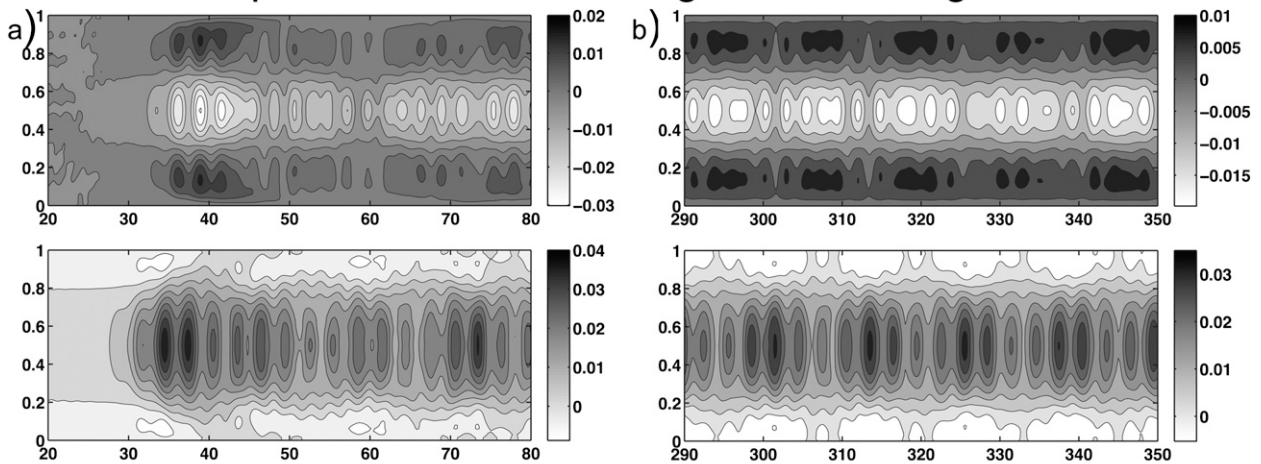
supercritical:  $g_0 = 0.6, h_0 = 0.1$ , and  $\sigma = 0.0$ . The plots are very similar to what we observed in Figs. 6a,b, because the mean shear is the same; the only difference is that there is also a relatively small periodic component. The main difference is that in Figs. 7a,b there is a combination of the natural frequency of oscillation and the frequency of the forcing. In contrast, Figs. 7c,d depict the equilibrated mean flows for the case with  $g_0 = 0.6, h_0 = 0.1$ , and  $\sigma = 1.0$  (i.e., moderate stochasticity in the baroclinic shear). The effect of the erratic variation is remarkable. The baroclinic adjustment creates barotropic and baroclinic zonal flows that are much stronger than in either the periodic or steady analogs. The magnitude of the baroclinic component is larger than the barotropic component

and is more than 10 times larger than what occurred in the periodic version. This implies that supercritical flows, as occur in the ACC, that have erratic variations can develop much stronger zonally corrected mean flows compared to what is found in either the steady or periodic counterparts. Therefore, the three essential ingredients to create this strong modulation are that the flow is supercritical, the amplitude of the time-dependent component is moderately strong, and the variations in the basic state are sufficiently erratic but not too erratic.

### 9. Conclusions

The Phillips model is an excellent paradigm in which to study large-scale geophysical shear flows, because it

### Equilibrated Mean Flow: $g=0.6$ $h=0.1$ $\sigma=0.0$



### Equilibrated Mean Flow: $g=0.6$ $h=0.1$ $\sigma=1.0$

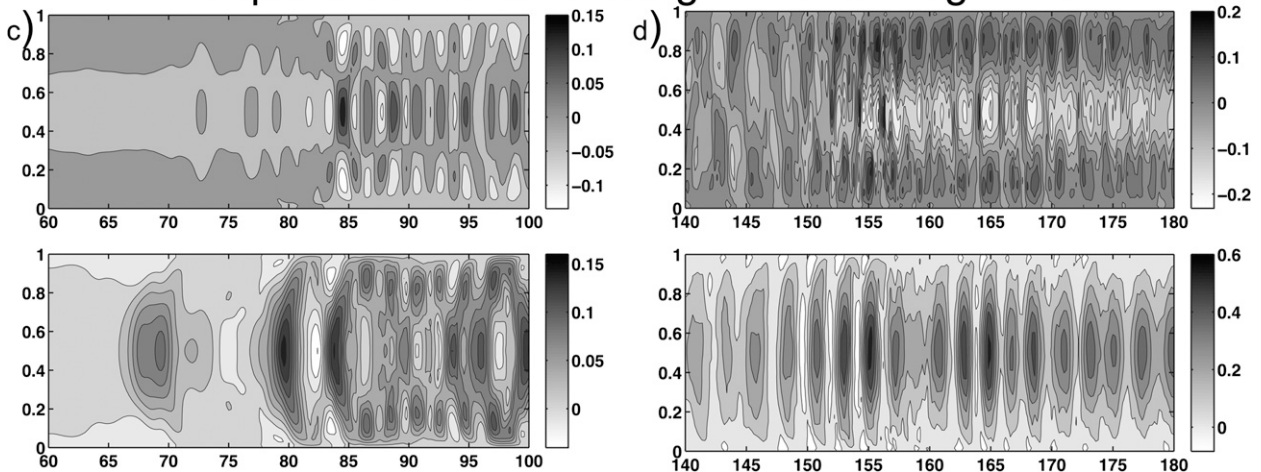


FIG. 7. As in Fig. 6, but focusing on an example where the basic state is periodic and has a mean shear that is slightly supercritical:  $g_0 = 0.6$ ,  $h_0 = 0.1$ , and  $\sigma = 0.0$ . (bottom) As in (top), but for an aperiodic basic state with  $g_0 = 0.6$ ,  $h_0 = 0.1$ , and  $\sigma = 1.0$ .

can display a wealth of different behaviors. It has long been known that the Phillips model can exhibit both barotropic and baroclinic instabilities when the steady shear has large enough gradients (Pedlosky 1987). Recently, Pedlosky and Thomson (2003) and Flierl and Pedlosky (2007) demonstrated that, if the basic state is periodic in time, then PI can occur. In this present work, we have studied the nonlinear evolution of steady, periodic, and aperiodic baroclinic shear to understand the effect of time dependency in the nonlinear regime. Our numerical simulations indicate the following: A temporally periodic vertical shear can further excite the barotropic component of the primary wave and the harmonics in comparison to a steady shear. Thus, even though parametrically unstable modes tend to grow more slowly in the linear regime, the baroclinic adjustment of these waves is more effective in generating the higher harmonics. We

have also found that, with an aperiodic baroclinic shear, the barotropic component of the primary wave can continue extracting energy from the mean flow, giving rise to a much stronger primary wave than in either the steady or periodic situations. Also, the higher harmonics can achieve a larger amplitude than what was observed in the periodic limit. Furthermore, aperiodicity of a time-dependent basic state whose mean is supercritical can have very strong corrections in the zonal mean flow. This signifies that the aperiodicity of the basic state plays a vital role in baroclinic adjustment of an unstable vertical shear. Presumably, this difference extends to the long time behavior of the adjustment process, but showing this result is beyond the scope of this work.

Our results suggest that care should be taken when considering data collected of oceanic currents. Because any oceanic dataset is necessarily sparse in both space

and time and always processed, the data are necessarily smoother than what actually transpired in the ocean. This filtering of noise can be very convenient to the modeler, but it yields that the data of the observed current are different in comparison to the real current. Our analysis of aperiodic baroclinic shear suggests that the linear stability of observed (databased with temporal variability removed, except perhaps for seasonal changes) oceanic flows is likely to be too large and that the amount of energy cascade is too small. Therefore, special attention should be given in parameterizing time-dependent shear flows, because their dynamics can be quite different in comparison to their time averages.

*Acknowledgments.* We thank all reviewers for their comments but one reviewer especially for great care in reading this manuscript. FJP was supported by NSERC and JP was supported by NSF OCE 0925061 during the research and writing of this manuscript.

#### REFERENCES

- Cai, M., 1992: An analytical study of the baroclinic adjustment in a quasigeostrophic two-layer channel model. *J. Atmos. Sci.*, **49**, 1594–1605.
- , and M. Mak, 1990: Symbiotic relation between planetary and synoptic scale waves. *J. Atmos. Sci.*, **47**, 2953–2968.
- Charney, J., and G. Flierl, 1981: Oceanic analogues of large-scale atmospheric motions. *Evolution of Physical Oceanography*, B. A. Warren and C. Wunsch, Eds., MIT Press, 504–549.
- Davis, S., 1976: The stability of time-periodic flows. *Annu. Rev. Fluid Mech.*, **8**, 57–74.
- Durski, S., R. Samelson, J. Allen, and G. Egbert, 2008: Normal-mode instabilities of a time-dependent coastal upwelling jet. *J. Phys. Oceanogr.*, **38**, 2056–2071.
- Farrell, B. F., and P. J. Ioannou, 1996: Generalized stability theory. Part II: Nonautonomous operators. *J. Atmos. Sci.*, **53**, 2041–2053.
- , and —, 1999: Perturbation growth and structure in time-dependent flows. *J. Atmos. Sci.*, **56**, 3622–3639.
- Flierl, G., and J. Pedlosky, 2007: The nonlinear dynamics of time-dependent subcritical baroclinic currents. *J. Phys. Oceanogr.*, **37**, 1001–1021.
- Gardiner, C., 2004: *Handbook of Stochastic Methods for Physics, Chemistry and the Natural Sciences*. Springer Series in Synergetics, Vol. 13, Springer-Verlag, 415 pp.
- Gille, S. T., and K. A. Kelly, 1996: Scales of spatial and temporal variability in the Southern Ocean. *J. Geophys. Res.*, **101**, 8759–8773.
- Gleeson, J., 2006: Phase diffusion due to low-frequency colored noise. *IEEE Trans. Circuits Syst.*, **53**, 183–186.
- Inoue, R., and W. Smyth, 2009: Efficiency of mixing forced by unsteady shear flow. *J. Phys. Oceanogr.*, **39**, 1150–1166.
- Klein, P., 1990: Transition to chaos in unstable baroclinic systems: A review. *Fluid Dyn. Res.*, **5**, 235–254.
- , and J. Pedlosky, 1986: A numerical study of baroclinic instability at large supercriticality. *J. Atmos. Sci.*, **43**, 1243–1262.
- Mak, M., 1985: Equilibration in nonlinear baroclinic instability. *J. Atmos. Sci.*, **42**, 2764–2782.
- Nowlin, W., and J. Klinck, 1986: The physics of the Antarctic Circumpolar Current. *Rev. Geophys.*, **24**, 469–491.
- Pedlosky, J., 1964a: The stability of currents in the atmosphere and ocean: Part I. *J. Atmos. Sci.*, **21**, 201–219.
- , 1964b: The stability of currents in the atmosphere and ocean: Part II. *J. Atmos. Sci.*, **21**, 342–353.
- , 1970: Finite-amplitude baroclinic waves. *J. Atmos. Sci.*, **27**, 15–30.
- , 1987: *Geophysical Fluid Dynamics*. 2nd ed. Springer-Verlag, 710 pp.
- , and L. M. Polvani, 1987: Wave-wave interaction of unstable baroclinic waves. *J. Atmos. Sci.*, **44**, 631–647.
- , and J. Thomson, 2003: Baroclinic instability in time-dependent currents. *J. Fluid Mech.*, **490**, 189–215.
- Phillips, N. A., 1951: A simple three-dimensional model for the study of large scale extra tropical flow patterns. *J. Meteor.*, **8**, 381–394.
- , 1954: Energy transformations and meridional circulations associated with simple baroclinic waves in a two-level, quasigeostrophic model. *Tellus*, **6**, 273–286.
- Pierrehumbert, R., 1995: Baroclinic instability. *Annu. Rev. Fluid Mech.*, **27**, 419–467.
- Poulin, F., 2010: The linear stability of aperiodic baroclinic shear. *J. Phys. Oceanogr.*, **40**, 568–581.
- , and G. Flierl, 2008: The stochastic Mathieu's equation. *Proc. Roy. Soc. London*, **464A**, 1885–1904.
- , —, and J. Pedlosky, 2003: The instability of time-dependent shear flows. *J. Fluid Mech.*, **481**, 329–353.
- Press, W. H., S. A. Teukolsky, W. T. Vetterling, and B. P. Flannery, 2007: *Numerical Recipes: The Art of Scientific Computing*. 3rd ed. Cambridge University Press, 1235 pp.
- Risken, H., 1984: *The Fokker-Planck Equation*. Springer-Verlag, 476 pp.
- Schmeits, M., and H. Dijkstra, 2001: Bimodal behavior of the Kuroshio and the Gulf Stream. *J. Phys. Oceanogr.*, **31**, 3435–3456.
- Shepherd, T., 1983: Mean motions induced by baroclinic instability of a jet. *Geophys. Astrophys. Fluid Dyn.*, **27**, 35–72.
- Stone, P., 1978: Baroclinic adjustment. *J. Atmos. Sci.*, **35**, 561–571.
- Talkner, P., L. Machura, M. Schindler, P. Hänggi, and J. Luczka, 2005: Statistics of transition times, phase diffusion and synchronization in a periodically driven bistable systems. *New J. Phys.*, **7**, 14–16.
- Van Kampen, N., 2001: *Stochastic Processes in Physics and Chemistry*. North Holland Personal Library, 465 pp.